



**HAL**  
open science

# A compact wide-scanning connected-slot array in a standard PCB for Ku/K/Ka-band applications

Syrine Hidri, Francesco Foglia Manzillo

► **To cite this version:**

Syrine Hidri, Francesco Foglia Manzillo. A compact wide-scanning connected-slot array in a standard PCB for Ku/K/Ka-band applications. EuMC 2023 - European Microwave Week, Sep 2023, Berlin, Germany. 10.23919/EuMC58039.2023.10290191 . cea-04328861

**HAL Id: cea-04328861**

**<https://cea.hal.science/cea-04328861>**

Submitted on 7 Dec 2023

**HAL** is a multi-disciplinary open access archive for the deposit and dissemination of scientific research documents, whether they are published or not. The documents may come from teaching and research institutions in France or abroad, or from public or private research centers.

L'archive ouverte pluridisciplinaire **HAL**, est destinée au dépôt et à la diffusion de documents scientifiques de niveau recherche, publiés ou non, émanant des établissements d'enseignement et de recherche français ou étrangers, des laboratoires publics ou privés.

# A Compact Wide-Scanning Connected-Slot Array in a Standard PCB for Ku/K/Ka-band Applications

Syrine Hidri<sup>#\*1</sup> and Francesco Foglia Manzillo<sup>#2</sup>

<sup>#</sup>CEA-Leti, Univ. Grenoble-Alpes, F-38000 Grenoble, France

<sup>\*</sup>Univ Rennes, CNRS, IETR (Institut d'Electronique et des Technologies du numéRique) - UMR CNRS 6164, F-35000 Rennes

{<sup>1</sup>syrene.hidri, <sup>2</sup>francesco.fogliamanzillo}@cea.fr

**Abstract** — We present a compact and cost-effective design of the unit-cell of a connected array of slots operating in Ku-, K- and Ka-band. A two-section hybrid superstrate directly loading the radiating aperture is proposed to achieve wide-angle impedance matching and enhanced cross-polarization discrimination. The first section is an artificial dielectric comprising three stacked subwavelength patch layers, two of which connected by vias, while the second one is an isotropic dielectric slab. This design comprises a reduced number of layers with respect to the state of the art, and enables an easier and robust fabrication of the antenna in a single standard printed circuit board. The simulated active VSWR is lower than 2.2 in a 3:1 bandwidth, within a scan range of  $\pm 60^\circ$  in all azimuthal planes. The numerical analysis of semi-infinite arrays with 16 elements proves that they can cover the same band in a field of view of  $\pm 50^\circ$  in the principal planes.

**Keywords** — phased array antennas, millimeter-wave antennas, antennas-in-package, broadband antennas.

## I. INTRODUCTION

Emerging applications such as satellite communications on the move and sixth-generation mobile networks are boosting the research on wide-angle scanning phased arrays operating over multiple bands with a single radiating aperture, up to millimeter-wave (mm-wave) frequencies. The realization of cost-effective and robust designs, suitable for low-loss integration with integrated circuits (ICs), is a key objective to enable their massive deployment. In the last decade, several ultra-wideband architectures have been proposed and demonstrated, mainly in the microwave spectrum. These arrays leverage on the high mutual coupling among their elements to attain aperture current distributions which are slowly varying with frequency, and comprise wide-angle impedance matching (WAIM) layers to enhance their field view. Tightly coupled dipole arrays (TCDAs) are usually realized using vertically oriented printed circuit boards (PCBs) [1], which hinders their integration in mm-wave front-ends. Alternative designs with tightly coupled dipoles, e.g. [2] and planar ultra-wideband modular arrays (PUMAs) [3], [4], can be fabricated using planar multilayer technologies, but often cover limited fields of view, e.g.  $\pm 45^\circ$  in elevation. On the other hand, connected arrays of slots, i.e. arrays of periodically excited long slots, attain unparalleled scanning performance when loaded by anisotropic WAIM superstrates [5]-[9]. Accurate models based on spectral methods have been presented [5], [6] and enable a fast design when the superstrate is realized using stacked subwavelength patches, also referred to as artificial dielectric layers (ADLs). Though this architecture is suited to

planar manufacturing, all designs reported in the literature, to the best of our knowledge, can be fabricated only by assembling multiple stacked PCBs. Indeed, the ADLs are realized on laminates and interleaved by foam spacers to maximize the field of view. With this approach, several unit-cells achieving bandwidths of 2.25:1 [6] to 10:1 [9] and field of views exceeding  $\pm 50^\circ$  have been reported. The  $16 \times 16$  prototype in [7] scans up to  $\pm 60^\circ$  and covers the 6-15-GHz band, with a uniform amplitude excitation. The superstrate includes 8 metal layers and 6 foam spacers, and the slots are realized on a drilled substrate.

In this paper, we present a cost-effective linearly polarized connected-slot array design which can be realized in a standard multilayer PCB. A hybrid two-section superstrate design, without any foam layer, is proposed. The first section is anisotropic and comprises 3 patch layers. The second one is an isotropic dielectric slab. The connected slot and the first section are realized using the same substrate material. The second section has slightly different material properties and can be thus easily bonded on the first. We numerically demonstrate that, despite the reduced number of metal layers and easier assembly process, the unit-cell scans up to  $\pm 60^\circ$  over a 3:1 bandwidth, from 11.9 GHz to 35.9 GHz. Moreover, an enhancement of the cross-polarization (X-pol) discrimination ( $>12$  dB) is attained by connecting two ADLs using vias, as originally proposed in [8]. Finally, the impact of finiteness effects on the performance are evaluated considering semi-infinite arrays of 16 elements.

## II. PRELIMINARY UNIT-CELL DESIGN

### A. Design methodology and matching performance

The proposed unit cell comprises a linearly polarized connected slot over a grounded substrate and a two-section WAIM superstrate placed above it, as shown in Fig. 1. The slot is excited by an ideal delta-gap feed for a preliminary cell optimization. The superstrate is designed using two equivalent quarter-wavelength transformers at the central frequency  $f_0 = 24$  GHz, which match the feed impedance, fixed at  $100 \Omega$ , to the impedance of free space. The effective relative permittivities of the two sections are 7.25 and 1.96, respectively. The first section is implemented using a three-layer uniaxial artificial dielectric. The transverse components of its permittivity tensor, under normal incidence, synthesize the required permittivity. All sheets are equal and comprise equi-spaced square subwavelength metal patches (see Fig. 1) in a host medium of relative permittivity  $\epsilon_{r1,h} = 2.2$ .

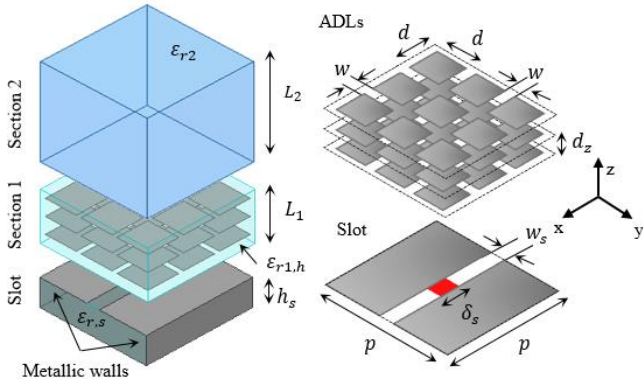


Fig. 1. Structure and main parameters of the preliminary unit-cell design.

The dimensions of the ADLs were iteratively optimized to fit the target effective permittivity using the procedure in [5]. The second section is a homogeneous dielectric slab of relative permittivity  $\epsilon_{r,2} = 1.96$ . This hybrid WAIM structure significantly reduces the number of metal layers and fabrication steps with respect to standard ADL-based designs. Once the WAIM is designed, the geometrical parameters of the radiating element were optimized to match its active input impedance to the feed impedance ( $100 \Omega$ ), for scan angles up to  $60^\circ$  in elevation, with the aid of a numerical tool. This tool implements the spectral Green's function model presented in [6]. A slab with relative permittivity  $\epsilon_{r,s} = \epsilon_{r,h}$  was selected as spacer between the radiating slot and the ground plane to ease the fabrication. Most designs [3], [7] use a lower effective permittivity, obtained by drilling substrates, to enhance the bandwidth. Metallic walls connect the metallic plane around the slot to the ground plane, to improve the scanning performance in the E-plane ( $yz$ -plane) [6]. The main dimensions of the cells are reported in Table 1. The array period  $p = 2.52$  mm is electrically smaller with respect to standard connected slot designs. The active VSWR plotted in Fig. 2 proves the wideband scanning performance. It is less than 2.6 between 12.8 GHz and 38.9 GHz, for scan angles up to  $60^\circ$  in the principal planes. The results obtained using the numerical tool are in tight agreement with full-wave simulations (Ansys Electronics Desktop).

### B. Improvement of cross-polarization performance

The ADL section in our design degrades the X-pol discrimination when scanning in the diagonal plane (D-plane,  $\phi = 45^\circ$ ), especially for large angles. Indeed, the ADL exhibits different effective refractive indexes,  $n_{TE}$  and  $n_{TM}$ , when illuminated by transverse electric (TE) and transverse magnetic (TM) waves, respectively. In particular,  $n_{TM}/n_{TE} = 1$  only at broadside and decreases with scan angle and frequency, as shown in Fig. 3a. These results were computed following [10] and using the scattering matrix obtained from a two-port full-wave simulation of the stand-alone ADL section. The maximum ratio in the matching band is 0.64 at  $60^\circ$ .

Table 1. Main dimensions of the preliminary unit-cell design in millimeters

$p$	$w_s$	$\delta_s$	$h_s$	$d$	$w$	$d_z$	$L_1$	$L_2$
2.52	0.3	0.3	0.65	$p/3$	0.11	$L_1/3$	1.16	2.23

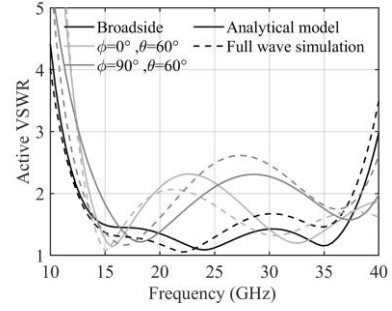


Fig. 2. Computed and simulated active VSWR of the preliminary cell design with a delta-gap feed, for three different beam-steering angles.

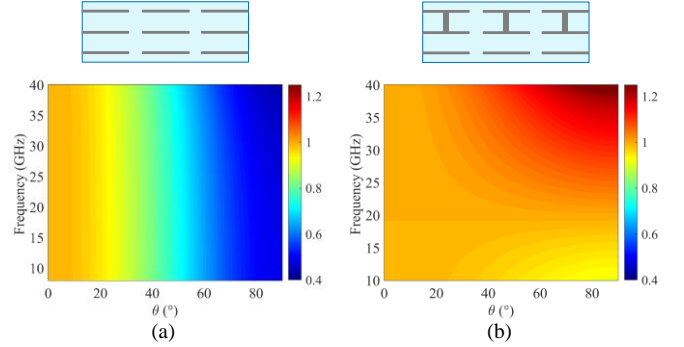


Fig. 3. Ratio  $(n_{TM}/n_{TE})^2$  for the stand-alone ADL section, as a function of frequency and scan angle: (a) without and (b) with vias.

The difference between  $n_{TE}$  and  $n_{TM}$ , at wide scan angles, and the X-pol level are larger when the ADL comprises low-permittivity spacers, e.g. foam layers [5]. The choice of  $\epsilon_{r,h} = 2.2$  in our design mitigates this issue. A further enhancement of the polarization purity is here achieved by connecting several stacked ADLs using vias, as in [8]. By doing so, only the  $z$ -component of the effective permittivity tensor significantly varies. Thus,  $n_{TM}$  can be increased, possibly up to approaching  $n_{TE}$ , which is instead essentially unaltered [8]. On the other hand, the increase of  $n_{TM}$  eases the onset of surface-waves, limiting the bandwidth. Several connections among the three patch layers of the ADL were analyzed via full-wave simulations to achieve the best trade-off between X-pol level and matching performance. The configuration where only the patches of the upper and middle layers are connected is retained (see Fig. 3b). In this case, the  $(n_{TM}/n_{TE})^2$  varies between 0.95 and 1.17 in the band, for scan angles up to  $60^\circ$ . The introduction of the vias slightly narrows the bandwidth for E-plane scanning. The X-pol component for a scan angle of  $60^\circ$  in the D-plane is reduced by 3 dB, as discussed in Section III.

## III. FINAL CELL DESIGN SUITABLE FOR PCB FABRICATION

### A. Stack-up optimization

The preliminary design described in Section II has been revisited to ensure its practical realization in a multilayer PCB using commercially available substrates and adhesive layers. This re-optimization has been carried out using the numerical model and thus neglecting the presence of the vias in the ADL. The modified stack-up and layer thickness are reported in Fig. 4a. The first superstrate section is realized using four Rogers

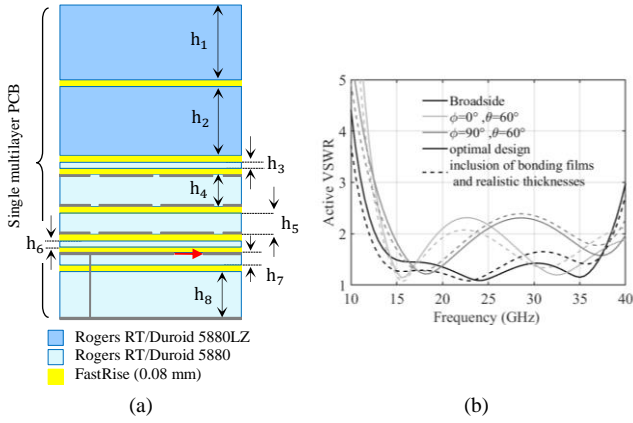


Fig. 4. (a) Unit-cell PCB stack-up ( $h_1 = h_2 = 1.026\text{mm}$ ,  $h_3 = h_6 = 0.068\text{mm}$ ,  $h_4 = 0.381\text{mm}$ ,  $h_5 = 0.252\text{mm}$ ,  $h_7 = 0.127\text{mm}$ ,  $h_8 = 0.508\text{mm}$ ). (b) Computed active VSWR with preliminary and final stack-up, for a delta-gap feed.

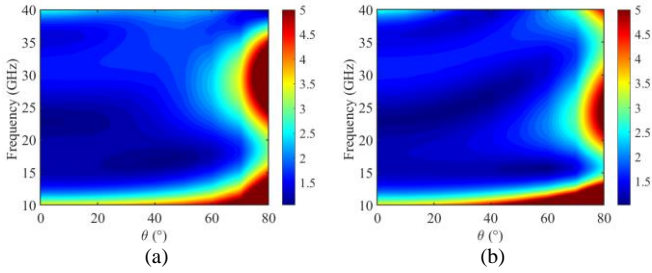


Fig. 5. Active VSWR of the unit-cell in Fig. 4a excited by an ideal feed, as a function of frequency and scan angle in the (a) E-plane; (b) H-plane ( $yz$ -plane).

RO5880 substrates ( $\epsilon_r = 2.2$ ). Two substrates of the same material are used to space apart the slot plane and the ground plane. The second section is instead implemented using two Rogers RO5880LZ substrates ( $\epsilon_r = 1.96$ ). Each pair of stacked substrates is bonded using  $80\text{-}\mu\text{m}$ -thick FastRise layers ( $\epsilon_r = 2.7$ ). The slot geometrical parameters were not varied (see Table 1). The active VSWR of the re-optimized cell, computed using the numerical tool, is plotted against frequency in Fig. 4b. Its behavior is very close to that of the preliminary design. It is  $<2.6$  from  $12.72\text{ GHz}$  to  $38.88\text{ GHz}$ , for scan angles of  $60^\circ$ . In this band, the peak VSWR values obtained scanning up to  $70^\circ$  in the E- and H-plane are  $2.9$  and  $3.5$ , respectively (see Fig. 5).

### B. Performance with the feeding structure

The final unit-cell stack-up is eventually obtained by introducing, in that shown in Fig. 4a, the vias in the ADL and the feed detailed in Fig. 6a. The slot is fed by a stripline with a series stub short-circuited to the ground plane of the slot. The stripline is excited through a circular aperture in the ground plane by a via, at  $0.46\text{ mm}$  from the via-fence wall connecting the slot plane to the ground. The proximity of feeding via to this wall makes the field propagation similar to that in an integrated coaxial feed [6]. The designed feed allows one to excite the slot using a microstrip network or an IC flip-chipped on an additional substrate underneath the ground plane. The unit-cell was excited using a port on the ground aperture, with a generator impedance of  $100\ \Omega$ . The simulated active VSWR is below  $2.5$  for steering at  $70^\circ$  and  $60^\circ$  in E- and H-plane,

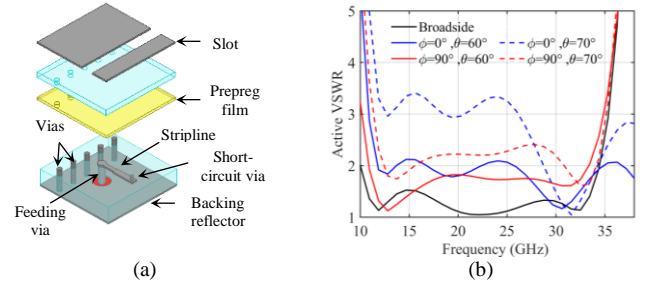


Fig. 6. (a) 3D view of the feeding structure (b) active VSWR of the final unit cell, excited by the designed feed, for different scanning angles.

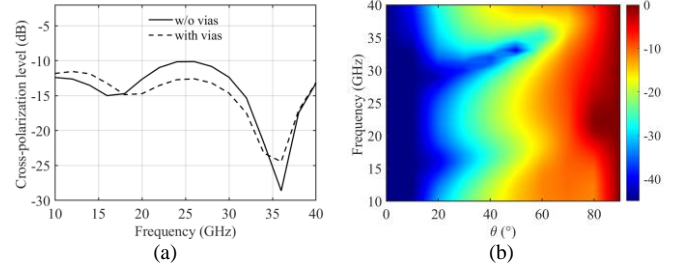


Fig. 7. X-pol level of the final unit-cell in the D-plane: (a) with and without vias in the superstrate, at  $60^\circ$ ; (b) as a function of frequency and scan angle.

respectively (see Fig. 6b). The X-pol level scanning at  $60^\circ$  in the D-plane is shown in Fig. 7a and compared to that obtained without vias in the superstrate. The X-pol is reduced by  $3\text{ dB}$  at  $f_0$  and remains  $<-12\text{ dB}$  in the entire band. The simulated X-pol level of the cell with the feed, in the D-plane, is plotted as a function of frequency and scan angle in Fig. 7b. The maximum values at  $60^\circ$  and  $70^\circ$  are  $-12\text{ dB}$  and  $-8.5\text{ dB}$ , respectively.

### IV. IMPACT OF FINITENESS ON THE ARRAY PERFORMANCE

The impact of the finiteness and edge effects on the scanning performance of a relatively small array is discussed. Semi-infinite arrays with  $16$  excited cells have been analyzed. In particular, a  $16 \times \infty$  array, i.e. an infinite array of finite slots, was simulated to evaluate the scanning capabilities in the H-plane ( $xz$ -plane). Similarly, an  $\infty \times 16$  array, i.e.  $16$  infinitely long and periodically excited slots, is considered to assess the scanning performance in the E-plane ( $yz$ -plane). In both cases, two dummy cells, terminated on matched loads, are added, one on each side of the finite array edge. In simulations, periodic boundary conditions are enforced along the direction where the array is infinite. Thus, the far-field patterns are computed considering that the lengths of the edges of the radiating apertures are  $45.36\text{ mm}$  and  $2.52\text{ mm}$ . In both arrays, the signals applied to the  $16$  excited elements have equal amplitudes and progressive phase shifts to steer the beam. The active VSWRs simulated at each element when the arrays steer at boresight and at  $50^\circ$  in the E- and H-planes are plotted Fig. 8a, b and c. The results obtained for the unit-cell are shown for comparison. The active VSWR is below  $3$  for most elements. The active VSWR of the central ( $8\text{th}$ ) elements of the arrays is shown in Fig. 8d. It is mostly  $<2.4$  from  $11.5\text{ GHz}$  to  $35.5\text{ GHz}$ , scanning up to  $50^\circ$ , except for a peak value of  $3.2$  observed at  $50^\circ$  in the H-plane. The co-polarized radiation patterns of the semi-infinite

## V. DISCUSSION AND CONCLUSION

We have presented the design of a linearly polarized connected-slot array cell which covers Ku-, K- and Ka-band (up to 35.9 GHz), and greatly reduces fabrication complexity and costs. The cell is loaded by a hybrid WAIM superstrate, including a first ADL section with 3 metal layers and a second one with dielectric slabs. The simulated active VSWR of the unit-cell is  $<2.2$  over a 3:1 bandwidth for scan angles up to  $70^\circ$  (E-plane) and  $60^\circ$  (H-plane). A semi-infinite array analysis demonstrates a scan coverage of  $\pm 50^\circ$  in the principal planes over the same band. Table 2 compares our design to unit-cells of state-of-the-art wide-angle scanning arrays. Simulated data are considered. Planar tightly-coupled arrays [2], [4] use less layers but achieve a smaller field of view and worse matching. With respect to similar connected-slot arrays [7], [8] the proposed design achieve a comparable scan range and a slightly wider bandwidth using a smaller number of layers. Moreover, it does not require special manufacturing steps, e.g. bonding of PCBs and foam spacers or substrate drilling. The small array pitch and the possibility to fabricate the proposed design in a robust, multilayer PCB is attractive for future integration with ICs.

## REFERENCES

- [1] E. Yetisir, N. Ghalichechian, and J. L. Volakis, "Ultrawideband array with  $70^\circ$  scanning using FSS superstrate," *IEEE Trans. Antennas Propag.*, vol. 64, no. 10, pp. 4256–4265, Oct. 2016.
- [2] M. H. Novak, F. A. Miranda, and J. L. Volakis, "Ultra-wideband phased array for millimeter-wave ISM and 5G Bands, realized in PCB," *IEEE Trans. Antennas Propag.*, vol. 66, no. 12, pp. 6930–6938, Dec. 2018.
- [3] S. Holland, D. Schaubert, and M. Vouvakis, "A 7–21 GHz dual-polarized planar ultrawideband modular antenna (PUMA) array," *IEEE Trans. Antennas Propag.*, vol. 60, no. 10, pp. 4589–4600, Oct. 2012.
- [4] J. T. Logan, R. Kindt, M. Lee, and M. Vouvakis, "A new class of planar ultrawideband modular antenna arrays with improved bandwidth," *IEEE Trans. Antennas Propag.*, vol. 66, no. 2, pp. 692–701, Feb. 2018.
- [5] D. Cavallo and C. Felita, "Analytical formulas for artificial dielectrics with nonaligned layers," *IEEE Trans. Antennas Propag.*, vol. 65, no. 10, pp. 5303–5311, Oct. 2017.
- [6] W. H. Syed, D. Cavallo, H. T. Shivamurthy, and A. Neto, "Wideband, wide-scan planar array of connected slots loaded with artificial dielectric superstrates," *IEEE Trans. Antennas Propag.*, vol. 64, no. 2, pp. 543–553, Feb. 2016.
- [7] D. Cavallo, W. H. Syed, and A. Neto, "Connected-slot array with artificial dielectrics: a 6 to 15 GHz dual-pol wide-scan prototype," *IEEE Trans. Antennas Propag.*, vol. 66, no. 6, pp. 3201–3206, Jun. 2018.
- [8] C. G. van Wamel, "Reduction of cross polarization level in connected slot arrays using artificial dielectric layers with vertical metallic inclusions," M. Sc. thesis, Delft University of Technology, Jul. 2022.
- [9] D. Cavallo, "Recent advances on wideband wide scanning connected slot arrays," *IEEE Int. Symp. Phased Array Syst. Techn. (PAST)*, Oct. 2022.
- [10] J. Cohen, R. Shavit, "Bi-anisotropic metamaterials effective constitutive parameters extraction using oblique incidence S-parameters method," *IEEE Trans. Antennas Propag.*, vol. 63, no. 5, pp. 2071–2078, May 2015.

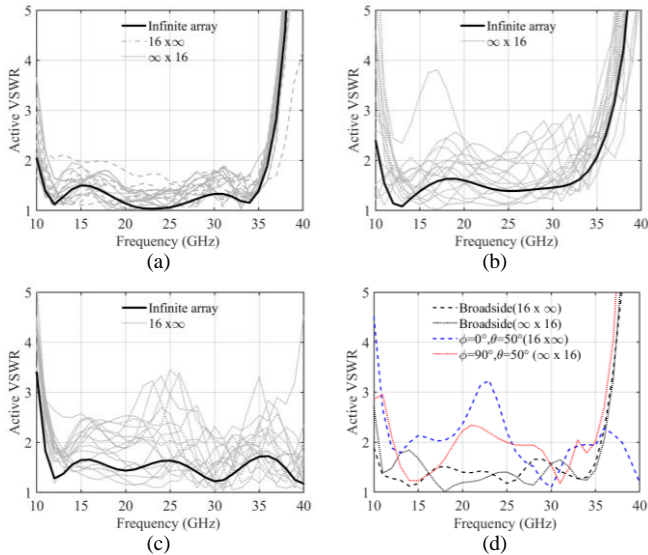


Fig. 8. Active VSWR of the semi-infinite arrays steering at: (a) boresight; (b)  $50^\circ$ , E-plane ( $\infty \times 16$ ); (c)  $50^\circ$ , H-plane ( $16 \times \infty$ ). (d) Active VSWR of a central element for these scan angles. Two dummy elements are included in each array.

arrays at 24 GHz are shown in Fig. 9, when steering at  $0^\circ$ , and at  $30^\circ$ , and  $50^\circ$  in the main planes. The patterns are normalized to the maximum radiated field of the broadside array. The theoretical scan loss, varying as the cosine of the scan angle, is also reported. When the arrays are phased for a nominal scan angle of  $50^\circ$ , they actually steer at  $48^\circ$ , due to their finiteness along the scan plane. The differences between the pattern values at  $48^\circ$  and  $50^\circ$  are  $<0.14$  dB. The simulated scan loss at  $50^\circ$  are 1.9 dB and 2.1 dB in the E- and H-plane, respectively. The H-plane half-power beamwidth (HPBW) is  $15.5^\circ$  and  $22.2^\circ$  when the  $16 \times \infty$  array scans at  $0^\circ$  and  $50^\circ$ , respectively. The HPBW of the boresight beam is  $10^\circ$  at 35.9 GHz.

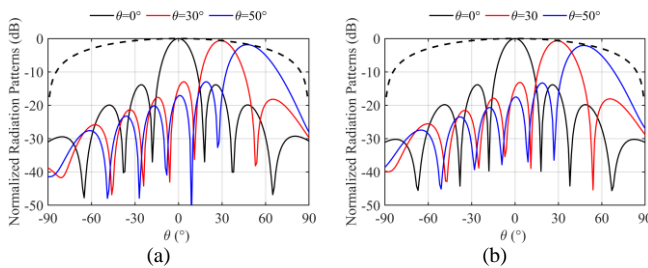


Fig. 9. Radiation patterns of the arrays at 24 GHz for 3 scan angles ( $0^\circ$ ,  $30^\circ$ ,  $50^\circ$ ) in (a) E-plane ( $\infty \times 16$ ) and (b) H-plane ( $16 \times \infty$ ). All patterns are normalized to the peak of the boresight beam. The theoretical scan loss is also shown.

Table 2. Comparison of the proposed design with state-of-the-art wideband wide-scanning array unit-cells

Design - Ref.	TCDA [2]	PUMA [3]	Connected slots [7]	Connected slots [8]	This work
Bandwidth / Active VSWR	24 - 72 GHz (3:1) VSWR $< 3$	7 - 21 GHz (3:1) VSWR $< 2.8$	6.8 - 14 GHz (2:1) VSWR $< 2.6$	11-32 GHz (2.9:1) VSWR $< 3.5$	11.9-35.9 GHz (3:1) VSWR $< 2.5$
Scan range	$\pm 45^\circ$ (E, H)	$\pm 45^\circ$ (E, H)	$\pm 75^\circ$ (E) / $\pm 60^\circ$ (H)	$\pm 60^\circ$ (E, H)	$\pm 70^\circ$ (E) / $\pm 60^\circ$ (H)
Polarization	Linear	Dual-linear	Dual-linear	Dual-linear	Linear
X-pol (D-plane)	n.a.	$< -15$ dB ( $45^\circ$ )	$< -7$ dB ( $60^\circ$ )	$< -6$ dB ( $60^\circ$ )	$< -12$ dB ( $60^\circ$ )
Size ( $^* \lambda_h^3$ )	$0.5 \times 0.5 \times 0.4$	$0.42 \times 0.42 \times 0.44$	$0.45 \times 0.45 \times 0.55$	$0.45 \times 0.45 \times 0.55$	$0.3 \times 0.3 \times 0.48$
Metal / foam layers	3 / 0	3 / 0	12 (8 ADLs) / 6	7 (4 ADLs) / 3	6 (3 ADLs) / 0

\* $\lambda_h$  is the wavelength in free space at the highest frequency of the reported band.